Observation of a threshold cusp at the $\Lambda \eta$ threshold in the pK^- mass spectrum with $\Lambda_c^+ \to pK^-\pi^+$ decays

S. B. Yang[®], K. Tanida[®], J. K. Ahn[®], I. Adachi[®], H. Aihara[®], D. M. Asner[®], H. Atmacan[®], V. Aulchenko[®], T. Aushev, R. Ayad, V. Babu, P. Behera, K. Belous, J. Bennett, M. Bessner, V. Bhardwaj, B. Bhuyan, D. Bodrov, J. Borah, A. Bozek, M. Bračko, P. Branchini, T. E. Browder, A. Budano, M. Campajola, D. Červenkov[®], M.-C. Chang[®], P. Chang[®], B. G. Cheon[®], K. Chilikin[®], H. E. Cho[®], K. Cho[®], S.-J. Cho[®], S.-K. Choi, Y. Choi, S. Choudhury, D. Cinabro, S. Das, G. De Pietro, R. Dhamija, F. Di Capua, Z. Doležal, T. V. Dong[®], D. Dossett[®], D. Epifanov[®], B. G. Fulsom[®], R. Garg[®], V. Gaur[®], A. Garmash[®], A. Giri[®], P. Goldenzweig, E. Graziani, T. Gu, Y. Guan, K. Gudkova, C. Hadjivasiliou, K. Hayasaka, H. Hayashii, W.-S. Hou, C.-L. Hsu, T. Iijima, K. Inami, N. Ipsita, A. Ishikawa, R. Itoh, M. Iwasaki, Y. Iwasaki, Y. Iwasaki, W. W. Jacobs[®], E.-J. Jang[®], Q. P. Ji[®], S. Jia[®], Y. Jin[®], K. K. Joo[®], K. H. Kang[®], G. Karyan[®], T. Kawasaki[®], H. Kichimi[®], C. Kiesling[®], C. H. Kim[®], D. Y. Kim[®], K.-H. Kim[®], Y. J. Kim[®], Y.-K. Kim[®], H. Kindo[®], P. Kodyš[®], T. Konno[®], A. Korobov[®], S. Korpar[®], E. Kovalenko[®], P. Križan[®], P. Krokovny[®], M. Kumar[®], R. Kumar[®], K. Kumara[®], Y.-J. Kwon[®], T. Lam[®], J. S. Lange[®], M. Laurenza[®], J. Y. Lee[®], S. C. Lee[®], C. H. Li[®], J. Li[®], L. K. Li[®], Y. Li[®], L. Li Gioi[®], J. Libby[®], K. Lieret[®], D. Liventsev[®], T. Luo[®], M. Masuda[®], T. Matsuda[®], D. Matvienko[®], S. K. Maurya[®], F. Meier[®], M. Merola[®], F. Metzner[®], K. Miyabayashi[®], R. Mizuk[®], G. B. Mohanty[®], I. Nakamura[®], T. Nakano, M. Nakao, Z. Natkaniec, A. Natochii, L. Nayak, M. Niiyama, N. K. Nisar, S. Nishida, H. Ono, P. Oskin[®], P. Pakhlov[®], G. Pakhlov[®], S. Pardi[®], H. Park[®], S.-H. Park[®], A. Passeri[®], S. Patra[®], S. Paul[®], T. K. Pedlar[®], R. Pestotnik, L. E. Piilonen, T. Podobnik, E. Prencipe, M. T. Prim, N. Rout, G. Russo, S. Sandilya, L. Santeljo, V. Savinovo, G. Schnello, J. Schuelero, C. Schwandao, Y. Seinoo, K. Senyoo, M. E. Sevioro, M. Shapkin[®], C. Sharma[®], C. P. Shen[®], J.-G. Shiu[®], J. B. Singh[®], A. Sokolov[®], E. Solovieva[®], M. Starič[®], M. Sumihama[®], T. Sumiyoshi[®], W. Sutcliffe[®], M. Takizawa[®], U. Tamponi[®], F. Tenchini[®], K. Trabelsi[®], T. Tsuboyama[®], M. Uchida[®], T. Uglov[®], Y. Unno[®], S. Uno[®], Y. Ushiroda[®], Y. Usov[®], R. van Tonder[®], G. Varner[®], A. Vossen, E. Waheed, E. Wang, M.-Z. Wang, X. L. Wang, M. Watanabe, S. Watanuki, O. Werbycka, E. Won, B. D. Yabsley, W. Yan, J. Yelton, J. H. Yin, C. Z. Yuan, Y. Yusa, Y. Zhai, Z. P. Zhang, V. Zhilich, and V. Zhukova

(Belle Collaboration)

(Received 1 September 2022; revised 6 January 2023; accepted 9 July 2023; published 16 August 2023)

We observe a narrow peaking structure in the pK^- invariant-mass spectrum near the $\Lambda\eta$ threshold. The peak is clearly seen in 1.5 million events of $\Lambda_c^+ \to p K^- \pi^+$ decay using the 980 fb⁻¹ data sample collected by the Belle detector at the KEKB asymmetric-energy e^+e^- collider. We try two approaches to explain this structure: as a new resonance and as a cusp at the $\Lambda\eta$ threshold. The best fit is obtained with a coherent sum of a Flatté function and a constant background amplitude with the reduced χ^2 of 257/243 (p=0.25), while the fits to Breit-Wigner functions are unfavored by more than 7σ . The best fit explains the structure as a cusp at the $\Lambda \eta$ threshold, and the obtained parameters are consistent with the known properties of $\Lambda(1670)$. The observation gives the first identification of a threshold cusp in hadrons from the spectrum shape.

DOI: 10.1103/PhysRevD.108.L031104

Regions around the mass thresholds of two hadrons have been of great interest for studies of exotic hadrons such as X(3872) and $P_c(4312)^+$ [1–3], which are found near mass thresholds of two hadrons. These near-threshold

Published by the American Physical Society under the terms of the Creative Commons Attribution 4.0 International license. Further distribution of this work must maintain attribution to the author(s) and the published article's title, journal citation, and DOI. Funded by SCOAP³.

resonances could appear as threshold cusps instead of usual smooth peaks with Breit-Wigner (BW) shape. A cusp, defined as a discontinuity in the derivative of spectrum function, always appears exactly at the threshold, and its position does not reflect the pole position of a resonance [4]. To understand the nature of a near-threshold behavior, it is necessary to identify whether the peak structure is a threshold cusp or usual peak of BW type. In principle, a threshold cusp can be distinguished from a smooth peak because the derivative diverges at the peak position, but practically, experimental mass resolution often makes such identification difficult [5]. Therefore, there are just a few cases where threshold cusp is identified [6–10], and none of them are from the spectrum shape.

In this paper, we report a newly discovered peaking structure in the pK^- mass spectrum near the $\Lambda\eta$ mass threshold [11]. A trace of this peak structure is observed in the previous analysis [12] of $\Lambda_c^+ \to pK^-\pi^+$ decay using a 980 fb⁻¹ data sample collected by the Belle Collaboration. A similar structure is also seen by LHCb in the same Λ_c^+ decay channel [13]. We approach this peak considering two possible cases: a BW-type peak and a visible $\Lambda\eta$ threshold cusp enhanced by the $\Lambda(1670)$ pole nearby.

If it is a BW-type peak, it suggests an existence of a new resonance. In this regard, two theory groups independently proposed a narrow Λ^* resonance with spin 3/2 near the $\Lambda\eta$ threshold [14,15] based on the $pK^- \to \Lambda\eta$ data [16], and the peak could be due to this Λ^* resonance in the $\Lambda_c^+ \to pK^-\pi^+$ decay as shown in Fig. 1(a). Such an exotic state is not expected in the quark model, and thus it is important to study the observed peak structure to see whether it is the case or not.

On the other hand, a visible cusp can arise via the $\Lambda\eta$ rescattering process in the $\Lambda_c^+ \to pK^-\pi^+$ decay as shown in Fig. 1(b). In this case, the $\Lambda(1670)$ could be involved in the S-wave $\eta\Lambda - pK^-$ rescattering. Therefore, the shape of the peaking structure is determined by the properties of $\Lambda(1670)$ such as partial widths of the $\Lambda(1670)$ into pK^- and $\eta\Lambda$ channels.

In this analysis, we use data collected by the Belle detector at the KEKB asymmetric-energy e^+e^- collider [17]. The data sample is taken at or near the $\Upsilon(nS)$ (n=1-5) resonances. The Belle detector is a large-solid-angle magnetic spectrometer consisting of a silicon vertex detector [18], a central drift chamber, an array of aerogel threshold Cherenkov counters, barrel-like arrangement of time-of-flight scintillation counters, and an electromagnetic calorimeter composed of CsI(Tl) crystals located inside a superconducting solenoid coil with a 1.5 T magnetic field. The detector is described in detail elsewhere [19].

We also use samples of $e^+e^- \rightarrow c\bar{c}$ Monte Carlo (MC) events to estimate reconstruction efficiencies and detector performance. The MC simulation samples are generated with PYTHIA [20] and EvtGen [21] and propagated by GEANT3 [22].

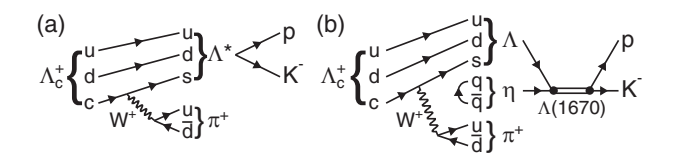


FIG. 1. Feynman diagrams for (a) a new Λ^* resonance and (b) a visible $\Lambda\eta$ threshold cusp enhanced by the $\Lambda(1670)$ pole in $\Lambda_c^+ \to pK^-\pi^+$ decay.

The same event selection criteria as in the previous $\Lambda_c^+ \to pK^-\pi^+$ analysis [12] are used to reconstruct the decay event from the charged p, K^- , and π^+ . The 1.5 × $10^6~\Lambda_c^+ \to pK^-\pi^+$ decays are reconstructed with the event selection criteria. For removing non- Λ_c^+ backgrounds, we subtract events in the signal range, 2.2746 < $M(pK^-\pi^+)$ < 2.2986 GeV/ c^2 , by events in the sideband ranges, 2.2506 < $M(pK^-\pi^+)$ < 2.2626 GeV/ c^2 and 2.3106 < $M(pK^-\pi^+)$ < 2.3226 GeV/ c^2 .

To improve the invariant-mass resolution on the $M(pK^-)$ distribution, three daughter particles of the decay are fitted to the common vertex point with the mass of Λ_c^+ . After this mass-constraint vertex fit, detector responses at 1663.5 MeV/ c^2 on the $M(pK^-)$ distribution can be represented by a double-Gaussian function with a common central mean value. From a MC simulation, standard deviations of the core and tail Gaussian functions are determined to be 1.25 MeV/ c^2 and 2.50 MeV/ c^2 , respectively, and the yield of the tail Gaussian function is 0.193 of the core Gaussian function.

We estimate the reconstruction efficiency of $\Lambda_c^+ \to pK^-\pi^+$ decay using the MC sample. Owing to variations of the estimated efficiencies on $M^2(K^-\pi^+)$ and $M(pK^-)$, we correct the Λ_c^+ yields in individual bins of the two-dimensional distribution of $M^2(K^-\pi^+)$ versus $M(pK^-)$ [23].

From the perspective of the pK^- peak as a usual hadron resonance structure, we perform a binned least- χ^2 fit to the efficiency-corrected $M(pK^-)$ distribution in the range of 1.54 GeV/ c^2 to 1.79 GeV/ c^2 with a nonrelativistic BW function defined as

$$\frac{dN}{dm} \propto |\mathrm{BW}(m)|^2 = \left| \frac{1}{(m - m_0) + i\frac{\Gamma_0}{2}} \right|^2, \tag{1}$$

where m, m_0 , and Γ_0 are the pK^- invariant mass, the nominal mass, and the resonance width, respectively [24]. The BW function is convolved with the double-Gaussian function with fixed parameters to take into account detector responses. The probability density function (PDF) for background Λ_c^+ decay events is a fifth-order Chebyshev polynomial function. Figure 2(a) shows the fit results using the BW function. The mass and width are obtained to be $1662.4 \pm 0.3 \text{ MeV}/c^2$ and $22.6 \pm 1.5 \text{ MeV}$, respectively, where the uncertainties are statistical. The reduced χ^2 is $1.35 \ (328/242)$.

A better reduced χ^2 is obtained by adding a complex constant to the nonrelativistic BW function coherently as $\frac{dN}{dm} \propto |\mathrm{BW}(m) + re^{i\theta}|^2$, where r and θ are real parameters, and θ is fixed to π , leading to constructive interference below the $\Lambda\eta$ threshold and destructive above that. Incoherent background Λ_c^+ decay events are represented by a third-order Chebyshev polynomial. Figure 2(b) shows the fit results, including the interference. The mass, width, and r are obtained as $1665.4 \pm 0.5 \ \mathrm{MeV}/c^2$, $23.8 \pm 1.2 \ \mathrm{MeV}$,

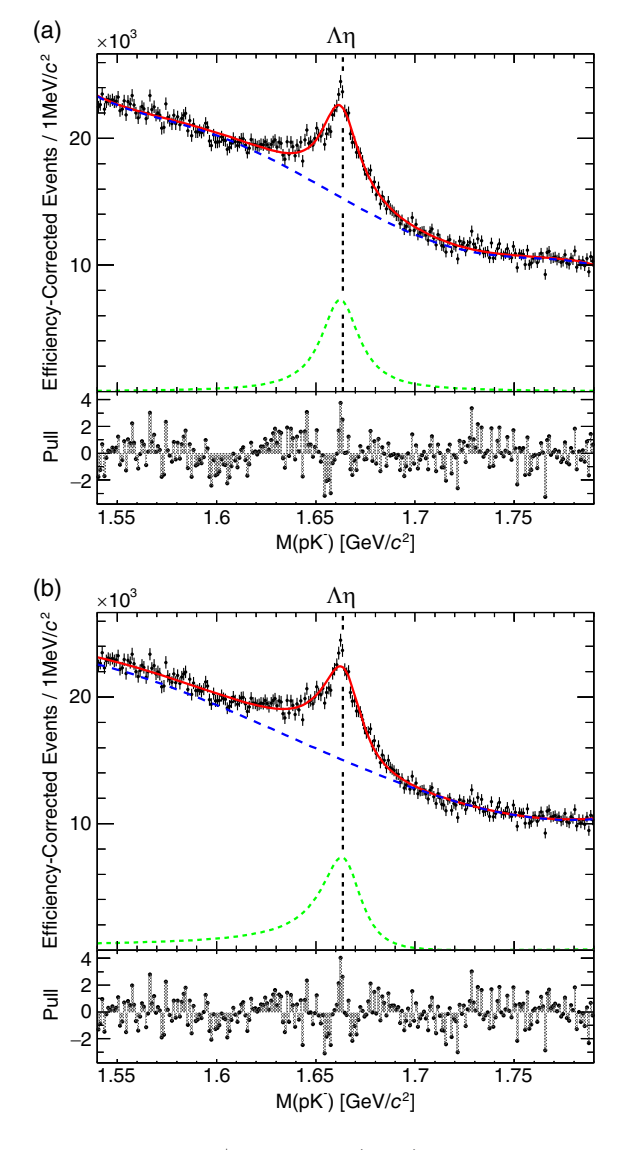


FIG. 2. Fits to the Λ_c^+ yield in $M(pK^-)$ spectra with (a) BW function and (b) BW model to which a complex constant is added. The curves indicate the full fit model (solid red), background Λ_c^+ decay events (long-dashed blue), (a) BW peak (dashed green), and (b) BW model with complex constant added coherently (dashed green). The $\Lambda\eta$ threshold is marked by the vertical dashed lines. The bottom panels show the pull distributions of the fits.

and $15.7 \pm 2.1~{\rm GeV^{-1}}$, respectively, where the uncertainties are only statistical, with the reduced χ^2 of 1.27 (308/243). Here, $re^{i\theta}$ represents an amplitude for the interference, and even if the r is changed to another BW function that represents nearby resonance, the fit results are consistent.

Another possibility is that the peak structure is a cusp at the $\Lambda \eta$ threshold enhanced by the $\Lambda(1670)$ pole nearby. We fit a nonrelativistic Flatté function [25,26] defined as

$$\frac{dN}{dm} \propto |f(m)|^2 = \left| \frac{1}{m - m_f + \frac{i}{2} (\Gamma' + \bar{g}_{\Lambda\eta} k)} \right|^2, \quad (2)$$

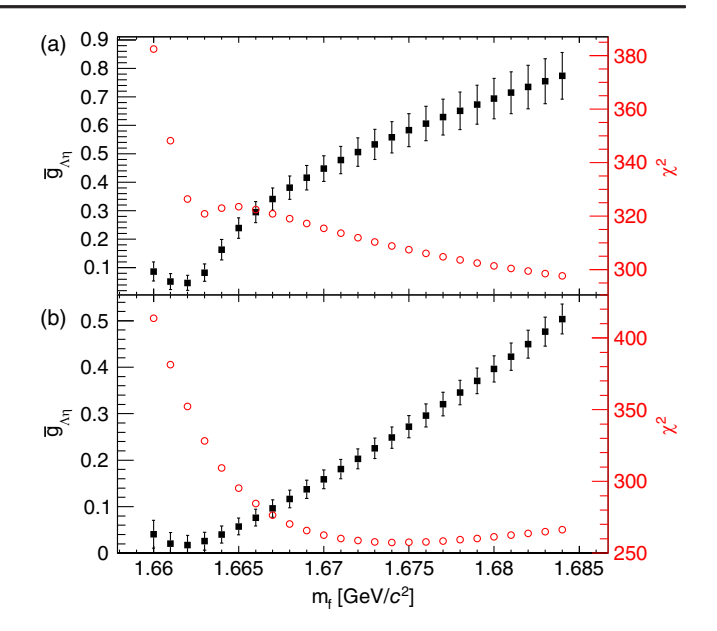


FIG. 3. $\bar{g}_{\Lambda\eta}$ and χ^2 from Flatté model (a) without and (b) with the interference as a function of fixed m_f . The black square and red circle markers indicate $\bar{g}_{\Lambda\eta}$ and χ^2 , respectively. Number of degree of freedom is 242 for all fits in (a) and 243 for all fits in (b). Uncertainty of $\bar{g}_{\Lambda\eta}$ is statistical.

to the peak region, where m is the pK^- invariant mass and m_f is a parameter corresponding to the nominal mass of $\Lambda(1670)$. The Γ' is a parameter for the sum of the partial widths of the decay modes other than $\Lambda\eta$, and is approximated as a constant in the following analysis. In the formula, $\bar{g}_{\Lambda\eta}k$ represents the partial decay width of the $\Lambda\eta$ channel, where $\bar{g}_{\Lambda\eta}$ and k are the dimensionless coupling constant and the decay momentum in the $\Lambda\eta$ channel, respectively. Here, k becomes imaginary below the $\Lambda\eta$ threshold so as to keep the analytic continuity. We also note that for $\bar{g}_{\Lambda\eta}=0$, Eq. (2) reduces to the BW function [Eq. (1)] with $m_f=m_0$ and $\Gamma'=\Gamma_0$.

Owing to the scaling behavior of the Flatté function [26], we fix m_f when we perform a fit and repeat the fit with various m_f values [5]. The signal PDF, Flatté function, is convolved with the double-Gaussian function for detector responses, and a fifth-order Chebyshev polynomial represents background Λ_c^+ decay events. Figure 3(a) shows the results on $\bar{g}_{\Lambda\eta}$ and χ^2 for each fixed m_f . A strong correlation between $\bar{g}_{\Lambda\eta}$ and m_f is seen as expected from the scaling. Typical fit results with fixed $m_f=1662.9~{\rm MeV}/c^2$ and $1674.4~{\rm MeV}/c^2$ are shown in Fig. 4.

The best fit is obtained by taking into account an interference with another S-wave amplitude such as a tail of $\Lambda(1405)$. We take a constant, $re^{i\theta}$, as the amplitude for these Λ_c^+ events, and add it to the Flatté coherently; here, θ is simply fixed to π to represent the Λ_c^+ events distribution, which drops rapidly above the $\Lambda\eta$ threshold, and variations from the fixed θ are considered as a source of systematic uncertainty.

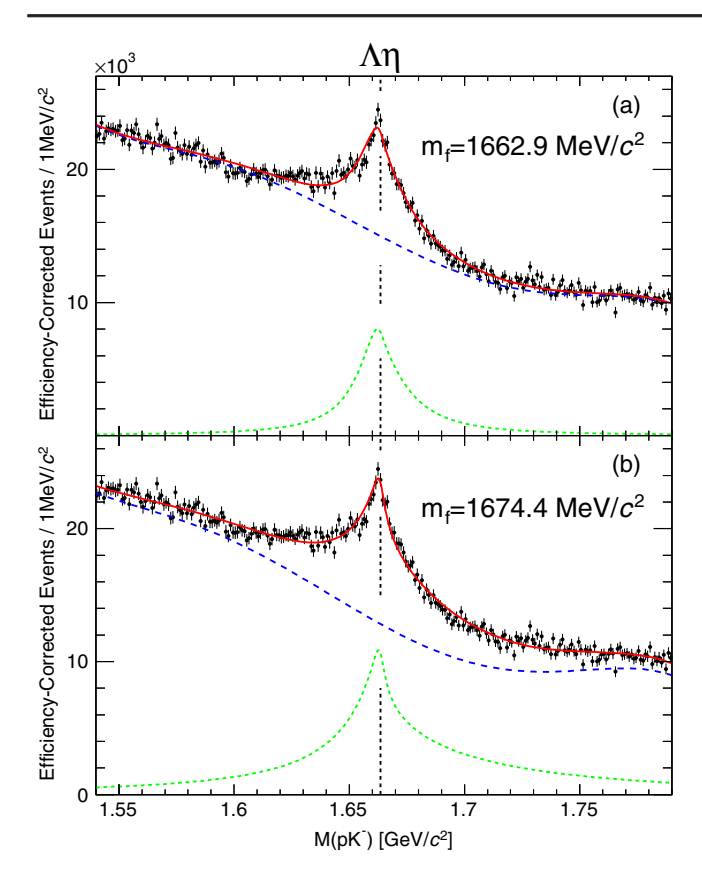


FIG. 4. Fits with Flatté function when m_f is fixed to (a) 1662.9 MeV/ c^2 and (b) 1674.4 MeV/ c^2 . The curves indicate the full fit model (solid red), Flatté function (dashed green), and background Λ_c^+ decay events (long-dashed blue).

We perform a binned least- χ^2 fit with the combined function, $\frac{dN}{dm} \propto |f(m) + re^{i\theta}|^2$, by changing the fixed m_f . Incoherent background Λ_c^+ decay events are represented by a third-order Chebyshev polynomial. As shown in Fig. 3(b), a strong correlation between m_f and $\bar{g}_{\Lambda\eta}$ is still seen even when the interference is taken into account. The best fit with the reduced χ^2 of 1.06 (257/243) is obtained at $m_f = 1674.4 \ \text{MeV}/c^2$, and the result is shown in Fig. 5. Γ' , $\bar{g}_{\Lambda\eta}$, and r are determined to be $27.2 \pm 1.9 \ \text{MeV}$, 0.258 ± 0.023 , and $29.2 \pm 3.4 \ \text{GeV}^{-1}$, respectively, where the uncertainties are only statistical. The partial width, $\Gamma_{\Lambda\eta}$, of the $\Lambda\eta$ channel is calculated as the product of $\bar{g}_{\Lambda\eta}$ and $q_{\Lambda\eta}^0$, which is the center-of-mass momentum of $\Lambda\eta$ at $m=m_f$. Then, the total width, Γ_{tot} , defined as a sum of Γ' and $\Gamma_{\Lambda\eta}$ is obtained to be $50.3 \pm 2.9 \ \text{MeV}$, where the uncertainty is only statistical.

We estimate the systematic uncertainties for $\bar{g}_{\Lambda\eta}$ and Γ' of the Flatté model with a constant added coherently. These systematic uncertainties are listed in Table I. We change the bin size of the $M(pK^-)$ distribution to 2 MeV to check the effect of binning. Systematic uncertainty from the mass resolution is estimated by increasing or decreasing the mass resolution by 20%. The effect of the absolute mass scaling

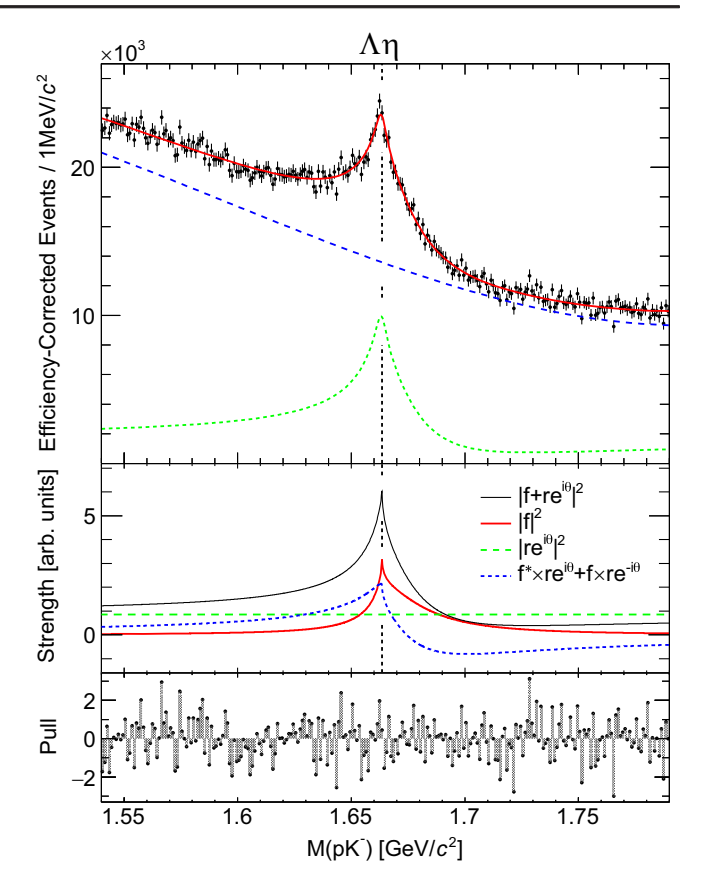


FIG. 5. Fit to the Λ_c^+ yield in $M(pK^-)$ spectrum with Flatté model to which a complex constant is added coherently with $m_f=1674.4~{\rm MeV}/c^2~{\rm and}~\theta=\pi$ being fixed. In the upper panel, the curves indicate the full fit model (solid red), Flatté function with complex constant added coherently (dashed green), and incoherent background Λ_c^+ decay events (long-dashed blue). The middle panel shows the breakdown for $|f+re^{i\theta}|^2$; the curves indicate the full function (thin solid black), $|f|^2$ (thick solid red), $|re^{i\theta}|^2$ (long-dashed green), and the interference term (dashed blue). The detector response is not taken into account. The bottom panel shows the pull distribution of the fit.

TABLE I. Systematic uncertainties in Γ' , $\bar{g}_{\Lambda\eta}$, and $\Gamma_{\rm tot}$ from Flatté fit for the pK^- peak structure.

Source	Γ' (MeV)	$\bar{g}_{\Lambda\eta}~(\times 10^{-3})$	Γ_{tot} (MeV)
Bin size	±0.0	±3	±0.3
Detector resolution	+0.3, -0.4	+7, -6	± 0.2
Absolute mass scale	± 0.8	+5, -6	± 1.3
Fit range	+1.1	-36	+0.8, -2.4
Efficiency correction	± 0.6	± 8	± 0.2
PDF model	+3.5, -4.9	+9, -29	+3.4, -6.4
θ	± 3.3	± 59	± 2.0
Interference	± 0.6	± 33	± 3.6
Total	+5.1, -6.0	+69, -82	+5.5, -8.1

is estimated by shifting the overall $M(pK^-)$ distribution by $\pm 0.2 \text{ MeV}/c^2$, which is a difference between a measured Λ_c^+ mass and the world-average value [27].

We vary the fit range to estimate the systematic uncertainty from the choice of the fit range. The same PDFs are used for fitting to a narrow range from 1.55 to 1.78 GeV/ c^2 . In the wide fit range from 1.48 to 1.8 GeV/ c^2 , the peak structure of $\Lambda(1520)$ appears and is represented by a D-wave relativistic BW function convolved with a double Gaussian function to represent detector responses. Background Λ_c^+ events are represented by a seventh-order Chebyshev polynomial. The largest differences in the fit results are considered as the systematic uncertainty from the fit range. A systematic uncertainty from the efficiency correction is estimated by performing a fit to the $M(pK^-)$ distribution without the efficiency correction. We repeat the fit with the θ set to free to estimate the systematic uncertainty from the fixed θ .

To estimate a systematic uncertainty due to the PDF modeling, we perform the fit with various PDFs. The PDF for the incoherent Λ_c^+ decay events is changed to secondand fourth-order Chebyshev polynomials. A D-wave relativistic BW function to represent a possible hidden peak structure of $\Lambda(1690)$ is added to the background PDF, and the yield ratio between $\Lambda(1670)$ and $\Lambda(1690)$ is varied from 0 to 1 according to Ref. [13]. We also change the nonrelativistic Flatté function to a relativistic form. In addition, we study a case where all the background Λ_c^+ decay events are coherent. The total PDF is changed to $|f(m) + \sqrt{(p_0 + p_1 m + p_2 m^2 + p_3 m^3)} e^{i\theta}|^2$, where p_i s (i=0,1,2, and 3) and θ are free parameters. The largest differences in the fit results of the PDF models are taken as the systematic uncertainty from the PDF model.

This one-dimensional fit strategy is validated with an amplitude analysis, which includes other resonances that can interfere with $\Lambda(1670)$, over the full-phase space, similarly to Ref. [13]. We conservatively account for the difference between the one-dimensional fit results and the amplitude analysis results, with Flatté model for $\Lambda(1670)$, as a source of systematic uncertainty. This systematic uncertainty, labeled interference in Table I, includes interference effects with higher partial waves.

In the Flatté fit, the reduced χ^2 is improved when the interference term is added, as it reproduces the drop of the background level around the peak structure. It indicates a significant interference with the background *S*-wave amplitude. Here we note that resonances in higher partial waves would not affect the cusp shape, because the discontinuity in the higher partial waves appears only in the second or higher derivatives, and the interference with *S*-wave vanishes with an integral over the solid angle. In addition, in both of the Flatté and BW cases, when events that do not overlap with $K^*(892)$ are selected in the $M^2(K^-\pi^+)$ range, the fit results are not significantly changed, meaning that the interference with $K^*(892)$ does not affect our conclusion [23].

The value of m_f that gives the best χ^2 is 1674.4 MeV/ c^2 , which is consistent with the recent measurement of $\Lambda(1670)$ mass, $1674.3 \pm 0.8 \pm 4.9$ MeV/ c^2 [28]. The total width at $m_f = 1674.4$ MeV/ c^2 is estimated as $50.3 \pm 2.9^{+5.5}_{-8.1}$ MeV and is also consistent with the recent measurement, $36.1 \pm 2.4 \pm 4.8$ MeV, within 1.4σ of the total uncertainty. In order to determine partial widths of $\Lambda\eta$ and pK^- and the Flatté parameters more accurately, a simultaneous-fit analysis with the $\Lambda(1670)$ peak structure in the $\Lambda\eta$ distribution is required.

The fit result with the Flatté function to which the constant is coherently added shows the best reduced χ^2 of 1.06 (257/243, p=0.25), in contrast to 1.27 (308/243, $p=3.1\times 10^{-3}$) from the best BW fit. In particular, the Flatté function reproduces the shape near the peak point better than the BW function. These results show that the present peaking structure is explained better by a threshold cusp than to a new hadron resonance by more than 7σ . This gives the first identification of a threshold cusp in hadrons from the spectrum shape. In the cusp interpretation, the structure near the $\Lambda\eta$ threshold is explained without the need of a new resonance. We also note that LHCb explained the structure using a BW function with fixed mass and width [13]. A small deviation is observed near the peak structure, but not considered to be significant.

This work, based on data collected using the Belle detector, which was operated until June 2010, was supported by the Ministry of Education, Culture, Sports, Science, and Technology (MEXT) of Japan, the Japan Society for the Promotion of Science (JSPS), and the Tau-Lepton Physics Research Center of Nagoya University; the Australian Research Council including Grants No. DP210101900, No. DP210102831, DE220100462, LE210100098, No. No. and LE230100085; Austrian Federal Ministry Education, Science and Research (FWF) and FWF Austrian Science Fund No. P 31361-N36; National Key R&D Program of China under Contract 2022YFA1601903, No. National Natural Science Foundation of China and research Grants No. 11575017, No. 11761141009, No. 11705209, No. 11975076, No. 12135005, No. 12150004, No. 12161141008, and No. 12175041, and Shandong Provincial Natural Science Foundation Project ZR2022JQ02; the Ministry of Education, Youth and Sports of the Czech Republic under Contract No. LTT17020; the Czech Science Foundation Grant No. 22-18469S; Horizon 2020 ERC Advanced Grant No. 884719 and ERC Starting Grant No. 947006 "InterLeptons" (European Union); the Carl Zeiss Foundation, the Deutsche Forschungsgemeinschaft, the Excellence Cluster Universe, and the VolkswagenStiftung; the Department of Atomic Energy (Project Identification No. RTI 4002) and the Department of Science and Technology of India; the Istituto Nazionale di Fisica Nucleare of Italy; National Research Foundation (NRF) of Korea Grants No. 2016R1-D1A1B-02012900, 2018R1-A2B-3003643, No. 2018R1-A6A1A-06024970, No. RS-2022-00197659, No. 2019R1-I1A3A-01058933, No. 2021R1-A6A1A-03043957, No. 2021R1-F1A-1060423, No. 2021R1-F1A-1064008, No. 2022R1-A2C-1003993; Radiation Science Research Institute, Foreign Large-size Research Facility Application Supporting project, the Global Science Experimental Data Hub Center of the Korea Institute of Science and Technology Information and KREONET/GLORIAD; the Polish Ministry of Science and Higher Education and the National Science Center; the Ministry of Science and Higher Education of the Russian Federation, Agreement 14.W03.31.0026, and the HSE University Basic Research Program, Moscow; University of Tabuk Research Grants No. S-1440-0321, No. S-0256-1438, and No. S-0280-1439 (Saudi Arabia); the Slovenian Research Agency Grants No. J1-9124 and No. P1-0135; Ikerbasque, Basque Foundation for Science, Spain; the Swiss National Science Foundation; the Ministry of Education and the

Ministry of Science and Technology of Taiwan; and the United States Department of Energy and the National Science Foundation. These acknowledgements are not to be interpreted as an endorsement of any statement made by any of our institutes, funding agencies, governments, or their representatives. We thank the KEKB group for the excellent operation of the accelerator; the KEK cryogenics group for the efficient operation of the solenoid; and the KEK computer group and the Pacific Northwest National Laboratory (PNNL) Environmental Molecular Sciences Laboratory (EMSL) computing group for strong computing support; and the National Institute of Informatics, and Science Information NETwork 6 (SINET6) for valuable network support. S. B. Yang and J. K. Ahn acknowledge the support provided by NRF Grant No. 2018R1A6A 3A01012138, No. 2018R1A5A1025563, No. 2019K1A3 A7A09034960, and No. 2021R1C1C2012925 and by the POSCO Science Fellowship of POSCO TJ Park Foundation. K. Tanida is supported by JSPS KAKENHI Grant No. 21H04478, and by the Reimei and Houga Research Programs of Japan Atomic Energy Agency.

- S.-K. Choi *et al.* (Belle Collaboration), Phys. Rev. Lett. 91, 262001 (2003).
- [2] R. Aaij et al. (LHCb Collaboration), Phys. Rev. Lett. 115, 072001 (2015).
- [3] R. Aaij *et al.* (LHCb Collaboration), Phys. Rev. Lett. **122**, 222001 (2019).
- [4] E. P. Wigner, Phys. Rev. 73, 1002 (1948).
- [5] R. Aaij et al. (LHCb Collaboration), Phys. Rev. D 102, 092005 (2020).
- [6] J. Batley *et al.* (NA48/2 Collaboration), Phys. Lett. B **633**, 173 (2006).
- [7] J. Batley *et al.* (NA48/2 Collaboration), Eur. Phys. J. C 64, 589 (2009).
- [8] V. L. Kashevarov *et al.* (A2 Collaboration at MAMI), Phys. Rev. Lett. **118**, 212001 (2017).
- [9] S. Acharya et al. (A Large Ion Collider Experiment Collaboration), Phys. Rev. Lett. 124, 092301 (2020).
- [10] F. Afzal *et al.* (CBELSA/TAPS Collaboration), Phys. Rev. Lett. **125**, 152002 (2020).
- [11] Unless stated otherwise, charge-conjugate modes are implied throughout this paper.
- [12] S. B. Yang *et al.* (Belle Collaboration), Phys. Rev. Lett. **117**, 011801 (2016).
- [13] (LHCb Collaboration), arXiv:2208.03262.
- [14] B.-C. Liu and J.-J. Xie, Phys. Rev. C 85, 038201 (2012).
- [15] H. Kamano, S. X. Nakamura, T.-S. H. Lee, and T. Sato, Phys. Rev. C 92, 025205 (2015).
- [16] A. Starostin *et al.* (The Crystal Ball Collaboration), Phys. Rev. C **64**, 055205 (2001).
- [17] S. Kurokawa and E. Kikutani, Nucl. Instrum. Methods Phys. Res., Sect. A 499, 1 (2003), and other papers included

- in this volume; T. Abe *et al.*, Prog. Theor. Exp. Phys. **2013**, 03A001 (2013), and references therein.
- [18] Z. Natkaniec *et al.* (Belle SVD2 Group), Nucl. Instrum. Methods Phys. Res., Sect. A 560, 1 (2006); Y. Ushiroda (Belle SVD2 Group), Nucl. Instrum. Methods Phys. Res., Sect. A 511, 6 (2003).
- [19] A. Abashian *et al.* (Belle Collaboration), Nucl. Instrum. Methods Phys. Res., Sect. A **479**, 117 (2002); J. Brodzicka *et al.* (Belle Collaboration), Prog. Theor. Exp. Phys. **2012**, 04D001 (2012).
- [20] T. Sjöstrand, S. Mrenna, and P. Skands, J. High Energy Phys. 05 (2006) 026.
- [21] J. Lange, Nucl. Instrum. Methods Phys. Res., Sect. A 462, 152 (2001); T. Sjöstrand, P. Edén, C. Friberg, L. Lönnblad, G. Miu, S. Mrenna, and E. Norrbin, Comput. Phys. Commun. 135, 238 (2001).
- [22] R. Brun et al., CERN Report No. DD/EE/84-1, 1984.
- [23] See Supplemental Material at http://link.aps.org/supplemental/10.1103/PhysRevD.108.L031104 for the efficiency correction and the fit results with the $M^2(K^-\pi^+)$ selection.
- [24] In equations, here and below, we use a natural unit that c equals 1.
- [25] S. M. Flatte, Phys. Lett. **63B**, 224 (1976).
- [26] V. Baru, J. Haidenbauer, C. Hanhart, A. Kudryavtsev, and U.-G. Meißner, Eur. Phys. J. A 23, 523 (2005).
- [27] P. Zyla et al. (Particle Data Group), Prog. Theor. Exp. Phys. 2020, 083C01 (2020).
- [28] J. Y. Lee *et al.* (Belle Collaboration), Phys. Rev. D 103, 052005 (2021).